Overview of results obtained at the Globus-M spherical tokamak

IOP Publishing and International Atomic Energy Agency Nuclear Fusion

Nucl. Fusion **49** (2009) 104021 (11pp) doi:10.1088/0029-5515/49/10/104021

Overview of results obtained at the Globus-M spherical tokamak

V.K. Gusev[1], S.E. Aleksandrov[1], V. Kh Alimov[2], I.I. Arkhipov[2], B.B. Ayushin[1], A.G. Barsukov[3], B. Ya Ber[1], F.V. Chernyshev[1], I.N. Chugunov[1], A.V. Dech[1], V.E. Golant[1], A.E. Gorodetsky[2], V.V. Dyachenko[1], M.M. Kochergin[1], G.S. Kurskiev[1], S.A. Khitrov[1], N.A. Khromov[1], V.M. Lebedev[4], V.M. Leonov[3], N.V. Litunovsky[5], I.V. Mazul[5], V.B. Minaev[1], A.B. Mineev[5], M.I. Mironov[1], I.V. Miroshnikov[6], E.E. Mukhin[1], Yu A. Nikolaev[1], A.N. Novokhatsky[1], A.A. Panasenkov[3], M.I. Patrov[1], M.P. Petrov[1], Yu V. Petrov[1], K.A. Podushnikova[1], V.A. Rozhansky[6], V.V. Rozhdestvensky[1], N.V. Sakharov[1], O.N. Shcherbinin[1], I. Yu Senichenkov[7], A.E. Shevelev[1], E.V. Suhov[7], I.N. Trapesnikova[1], E.I. Terukov[1], G.N. Tilinin[3], S. Yu Tolstyakov[1], V.I. Varfolomeev[1], A.V. Voronin[1], A.P. Zakharov[2], R. Kh Zalavutdinov[2], V.A. Yagnov[8], E.A. Kuznetsov[8] and E.G. Zhilin[9]

[1] Ioffe Physical-Technical Institute of the Russian Academy of Sciences, St Petersburg, Russia
[2] A.N. Frumkin Institute of Physical Chemistry and Electrochemistry, Russian Academy of Sciences, Moscow, Russia
[3] NFI RRC 'Kurchatov Institute', Moscow, Russia
[4] B.P. Konstantinov Nuclear Physics Institute, Russian Academy of Sciences, Gatchina, Russia
[5] D.V. Efremov Institute of Electrophysical Apparatus, St Petersburg, Russia
[6] Saint Petersburg State Polytechnical University, St Petersburg, Russia
[7] Saint Petersburg State University, St Petersburg, Russia
[8] State Research Center of Russian Federation, TRINITI, Moscow region, Troitsk, Russia
[9] Ioffe Fusion Technologies Ltd., St Petersburg, Russia

E-mail: vasily.gusev@mail.ioffe.ru

Received 11 December 2008, accepted for publication 8 April 2009
Published 10 September 2009
Online at stacks.iop.org/NF/49/104021

Abstract
Experiments and simulations to achieve high values of plasma parameters at the Globus-M spherical tokamak (ST) at moderate absolute auxiliary heating power (up to 0.8 MW) and high specific heating power (up to 2–3 MW m^{-3}) are described. Important distinguishing features are the low edge safety factor range, which is unusual for STs, $2.7 < q < 5$ and small plasma–outer wall space (3–5 cm). High ion heating efficiency with neutral beam injection (NBI) was demonstrated. Results of numerical simulation of fast ion trajectories are described and fast ion generation during the NBI and ion cyclotron resonance heating is discussed. Investigations on their confinement and slowing down are also presented. Reasons for achievement of high IC heating efficiency are outlined. Reliable H-mode regime achievement is described. Transport ASTRA modelling demonstrated that during NB heated H-mode ion heat diffusivity remains neoclassical and the particle diffusion coefficient inside transport barrier decreases significantly. Analysis was performed of divertor tile and special probe surfaces after irradiation by plasma during a large number of shots (3000–10 000 shots). Mixed layer composition is measured and deuterium retention in different tokamak first wall areas is estimated. Plasma jet injection experiments with upgraded plasma jet are described. Jet penetration to the plasma centre with immediate increase of density and temperature drop is proved and analogy with pellet injection is outlined.

PACS numbers: 52.55.Fa

1. Introduction

Globus-M is one of the modern spherical tokamaks (STs) concentrating its programme onto the most significant branches of hot temperature plasma research, with application to fusion devices. Detailed attention is devoted to the development of plasma auxiliary heating methods, investigation of heating physics, transport and plasma MHD stability. Diagnostics and fuelling tool development, investigation of plasma–wall interaction aimed at material research and creation of the basis for non-inductive CD and divertor physics research in ST are also important parts of the research programme. Basic Globus-M features and basic results could be found in [1–9].

The paper is focused on an overview of the main results achieved on Globus-M during the last 2 y. During the reported period further improvement of the device performance has been made. Basic efforts were devoted to increase in target plasma parameters, neutral beam injection (NBI) system improvement, heating physics clarification in ST conditions, H-mode study, development of diagnostics, investigation of plasma–wall interaction products and deuterium retention, and the upgrade of the plasma jet injection method for tokamak fuelling purpose. This paper contains, in section 4.3, corrected values for the deuterium content of carbon surfaces exposed to the plasma, originally presented in the preprint [10].

2. Plasma auxiliary heating and fast ion confinement

The basic plasma auxiliary heating method in Globus-M is the NBI of deuterium or hydrogen atoms. Typical NB parameters are 0.3–0.8 MW of beam power and 20–29 keV of beam energy [9, 11]. The NB heating physics in ST conditions was studied on a few machines only [12–14] and requires further clarification. The second auxiliary heating method is the ion cyclotron resonance heating (ICRH) in a frequency range corresponding to the fundamental harmonic of a hydrogen minority in deuterium plasma. Such a method is under test on STs for the first time. Typical ranges of ICR parameters are frequency 7–9 MHz and power 0.1–0.3 MW [6].

The heating experiments on Globus-M have an important difference as compared with other STs. At first Globus-M is a small dimension tokamak: the plasma major radius is $R \sim 0.36$ m, the minor radius, $a \sim 0.24$ m, the aspect ratio, $A = R/a \sim 1.5$, the plasma vertical elongation $\kappa \sim 1.5$–2. Due to strong toroidicity the toroidal magnetic field changes along the major radius from 1.1 to 0.23 T from the inner to the outer border. The typical NB footprint is comparable with the plasma cross section. Also the vacuum wavelength of the heating wave excited by the antenna loop during ICRH exceeds the plasma dimensions. Moreover, in these conditions, fast particle orbits span most of the plasma region. Such complications make the investigation of heating physics of primary importance. In addition, the specific heating power launched into discharge can reach a high value of 2–3 MW m^{-3} in Globus-M. Lastly, experiments in Globus-M are normally conducted with a small plasma–outer wall gap of 3–5 cm and in an edge safety factor range $2.7 < q_{95} < 5$ ($0.8 < q_{cyl} < 1.4$), which is unusually low for STs.

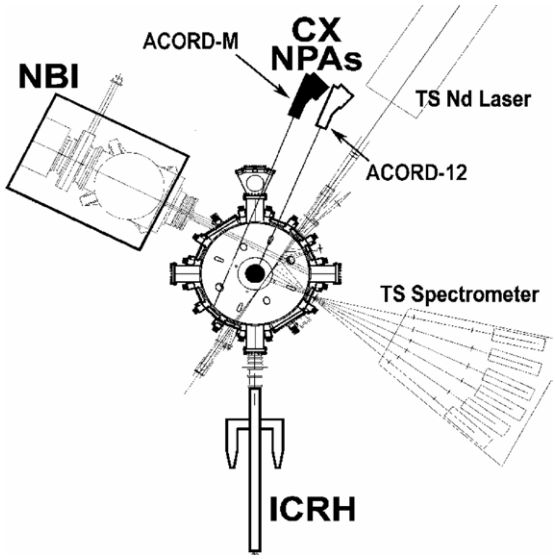

Figure 1. Apparatus arrangement at the Globus-M tokamak.

2.1. NBI heating

During the NB heating investigation fast ion performance was studied by charge-exchange (CX) diagnostics. The diagnostics consist of two neutral particle analyzers (NPA) of the ACORD type [15]. The equipment arrangement is shown in figure 1.

Chosen NPA arrangement provided data about trapped ions ($\perp$ NPA ACORD-12), as well as about passing ions (// NPA ACORD-M) and made possible study of fast ions generated during the NB and ICRH experiments [16]. The direct losses (shine-through and first-orbit losses) of the NB particles are calculated to be significant in low density plasmas as a result of the small plasma size and low magnetic field. For example for typical Globus-M plasma ($I_p = 200$ kA, $B_T = 0.4$ T) with $\langle n_e \rangle \sim 3 \times 10^{19}$ m^{-3} the estimated level of direct losses of 20 keV D-ions is about 50% (~20% of shine-through and ~30% of first-orbit losses). Experiments to study deceleration physics of NB produced fast ions were performed. The slowing down energy spectra measured during the NB co-injection into deuterium plasma are shown in figure 2. Solid curves correspond to the theoretical prediction of slowing down due to Coulomb collisions based on the analytical solution of simplified zero-dimensional Fokker–Planck equation [17], normalized to the NPA data at energies 4–9 keV. Particle flux steps at energies $E_b/2$ and $E_b/3$ are clearly defined. Direct losses were estimated on the basis of beam particle trajectory simulations [18] and were taken into account. The magnetic field geometry was reconstructed from magnetic measurements with the EFIT code [19]. The spectra waveforms (figure 2) correspond well to the fundamental Coulomb collision slowing down process with corrections to the direct beam ion loss prediction (20% for H-beam and 40% for D-beam).

In spite of the difficulties mentioned above and relatively high beam ion losses predicted at low target plasma densities [11], high ion heating efficiency was demonstrated in Globus-M. With NB power $P_{NB} = 0.8$ MW and $E_b = 25$ keV ion temperature increased ~3.5 times from the OH value and reached 0.75 keV during the NBI (figure 3).

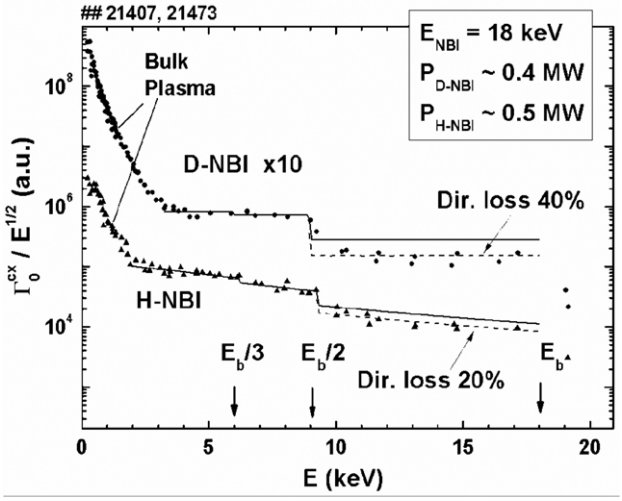

Figure 2. Slowing down energy spectra measured during H-NBI and D-NBI. Plasma conditions: D-plasma, $I_p = 180$ kA, $B_T = 0.4$ T, $\langle n_e \rangle \sim 4 \times 10^{19}$ m^{-3}, $T_e \sim 500$ eV. Characteristic slowing down time of fast ions on electrons is about 24 ms for D-ions and 12 ms for H-ions. The calculated slowing down spectrum is shown without (solid line) and with (dashed line) correction for the estimated direct losses of the full energy component from the injected neutral distribution.

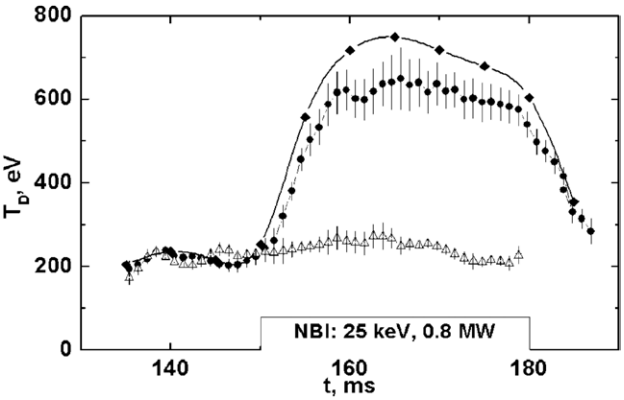

Figure 3. Record central ion temperature during D-NBI heating in Globus-M. ●—Measured by NPA ACORD-12, ♦—corrected to plasma opacity, Δ—ion temperature in reference OH discharge. Plasma conditions: non-shifted D-plasma, $I_p = 180$ kA, $B_T = 0.4$ T, $\langle n_e \rangle = 2.5$ m^{-3}, $T_e \sim 500$ eV.

In this experiment the ion temperature is ~1.5 times greater than electron temperature. Later on the experiment with 'hot' ions (i.e. $T_i > T_e$) was repeated in other conditions. Direct beam orbit losses were decreased due to the shift of plasma column towards the inner wall by ~5 cm. The ion temperature increase during shifted plasma NB heating is about 2.5 times higher than in normal (non-shifted) column [16]. Numerical orbit simulation shows that the NB generated fast D^+ ions with the energy up to 25 keV could be currently confined inside a wide region of plasma in Globus-M. The maximal energy of confined ions during co-injection is limited in conditions of Globus-M (plasma current 200 kA) by high energies ~50 keV. However high energy ions are confined in quite a narrow zone and experience high losses outside it [20] and further optimization of the NB heating in Globus-M is desirable. Nonetheless, the NB heating produces high energy content and improves MHD stability of Globus-M plasma

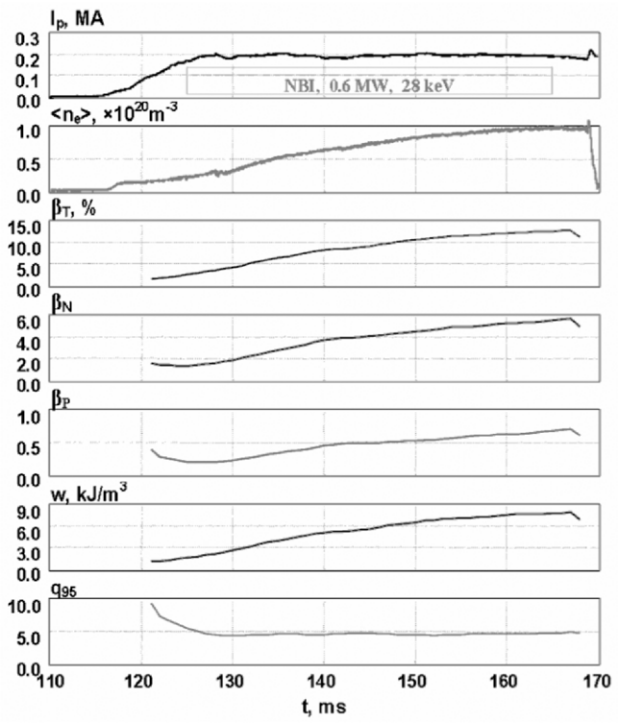

Figure 4. Temporal evolution of plasma parameters in the Globus-M shot with record values of stored energy and beta normalized. From top to bottom: I_p—plasma current, $\langle n_e \rangle$—line averaged density, β_T—toroidal beta, β_N—normalized beta in % m T MA^{-1}, $w = W_{tot}/V$, where W_{tot} is the total plasma energy and V is the plasma volume, q_{95}—safety factor at the 95% normalized poloidal flux surface. The data for beta, W, V and q are calculated by EFIT using external magnetic data [27].

against locked modes, connected with error fields possibly due to additional toroidal plasma rotation.

Temporal evolution of plasma parameters in one of the record shots for Globus-M is shown in figure 4.

2.2. Ion cyclotron heating

The ICRH experiments at the fundamental harmonic of light atomic mass (hydrogen) minority in deuterium plasma were performed in the Globus-M ST. This heating scheme was used in STs for the first time. A wide range of 'minority' concentration (n_H) in deuterium plasma, $C_H = n_H/(n_H + n_D) \approx$ 10–75%, is a specific feature of Globus-M experiments. Experiments with single loop antenna launcher, exciting a broad spectrum ($N < 150$), were performed and results were compared with numerical simulations of fast magnetosonic wave propagation and absorption in Globus-M [6]. It has been found that under optimized experimental conditions, which require displacement of the second harmonic resonance beyond the launcher, the presence of reflecting walls, surrounding plasma and a large fraction of the power launched into the short wavelength part of the antennae spectrum, the heating efficiency is high enough. Doubling of ion temperature at 200 kW of launched power could be achieved at high 'minority' concentration up to $C_H = 75\%$ [6].

The absorption of fast magnetosonic (FMS) waves in plasma is accompanied by generation of hydrogen suprathermal ions. CX energy spectrum analysis of light

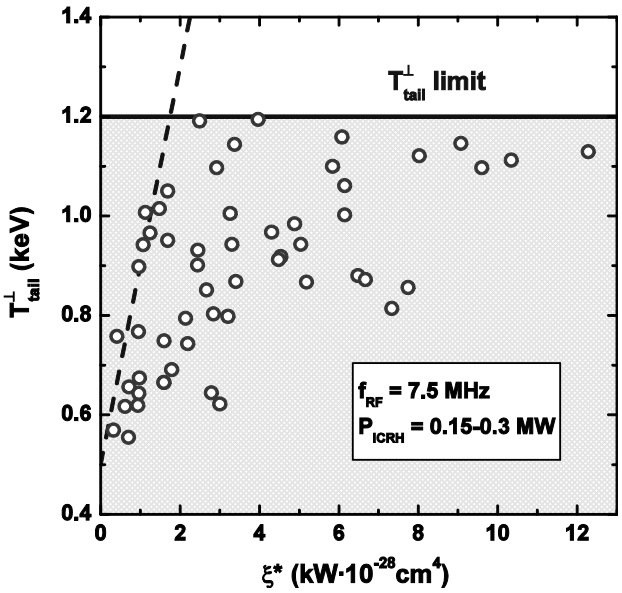

Figure 5. ICRH 'tail' temperature dependence, obtained using $\perp$ NPA measurements, on the specific power deposition per single particle. Dashed line—theory 'tail' temperature dependence, solid line—experimentally observed 'tail' temperature limit.

atomic mass minority (hydrogen), obtained by $\perp$ NPA, reveals that it consists of two parts. One represents the thermal part and the other one is the so called high energy tail. Due to the tail slope one could define the tail 'temperature'. According to the classic ICRH theory, developed for conventional tokamaks, the tail temperature is linearly dependent on Stix parameter [21, 22]. This is not the case during ICRH in ST. In our experiments the RF power input per single particle ($\xi^* = P_{\mathrm{ICRH}}/(C_{\mathrm{H}}(nl)^2)$, where P_{ICRH} is ICRH power, nl is line density and ξ^* is roughly the Stix parameter) was changed by the factor of 25. At the same time the tail temperature changed only by a factor of two and remained below 1.2 keV. The experimental data are presented in figure 5.

The dashed line shows theoretical prediction for conventional tokamak, $T_{\mathrm{tail}}^{\perp} = T_{\mathrm{e}} + 0.4\xi^*$, the solid one is the experimental limit in the case of Globus-M. It indicates that the RF power absorbed by minority ions from the tail is limited. We assumed that this limitation was connected with finiteness of energy of accelerated minority ions. In other words the minority ions undergo first-orbit losses if they exceed some maximal energy E_{max}. Using the observation of CX flux decay after RF termination, the maximal energy of accelerated protons was estimated as $E_{\mathrm{max}} \sim 15$ keV [16]. To prove the experimental data the trajectory simulations of minority ions in the Globus-M magnetic field, reconstructed using the EFIT code, were performed. Figure 6 demonstrates the fast ion banana orbit (left) and the map of banana orbit tip positions for different E_{max} (right). Fat solid oval line indicates the plasma last closed flux surface (LCFS). Line labelled by ω_H shows the position of the cyclotron resonance for the hydrogen fundamental harmonic. This map could be regarded as confinement zones of fast protons born with different energies in Globus-M poloidal cross section. As can be seen E_{max} is about 15 keV for protons having the banana orbit tips near the fundamental harmonic region. This correlates well with the value estimated from the experiment. One should keep in mind that in the Globus-M condition a considerable part of FMS wave power can be transmitted to plasma ions without producing ion tails through Bernstein wave conversion. This may partly explain the heating efficiency increase especially at higher hydrogen concentration.

3. High plasma confinement regime

Reliable transition into high confinement regime (H-mode) was achieved in Globus-M after change in the toroidal magnetic field direction. The toroidal magnetic field became parallel to the plasma current direction. Ion ∇B drift is directed towards the lower X-point, which is usually placed inside the vacuum vessel. L–H transition is recorded in OH regime, as well as in NB and IC heating regimes both in limiter and divertor configurations. Different events could trigger the H-mode (MHD, gas puff, etc) [23]. The change in the toroidal magnetic field direction also improved the plasma performance in the L-mode. The transport analysis of H-mode discharges was started with the help of 1D ASTRA code (details are given below). In spite of the preliminary character of the results they may be useful for ST transport process understanding and comparison with the results from other tokamaks.

3.1. Ohmic H-mode

Temporal evolution of plasma parameters in ohmic H-mode, shot #18083, is shown in figure 7. The L–H transition is triggered spontaneously in this discharge. In the phase of the transition the OH power does not exceed 0.3 MW. The H-mode phase of the discharge demonstrated almost all typical features, including a reduction in D-alpha emission and a simultaneous rise in plasma density which continued in the absence of external gas puffing. If the L–H transition occurs in the conditions of intense gas puffing providing fast density rise H-mode visible characteristic features could be smeared. Ohmic shot #21987 with intense density rise was chosen for transport analysis. The L–H transition is followed by the formation of a steep gradient in the electron density profile near the separatrix and a flat density distribution over the plasma volume.

Experimentally measured values of the plasma ion and electron temperatures, density and plasma loop voltage were used as the input parameters for the 1D ASTRA code simulations [24]. The transport model is described in [25]. The ion thermal diffusivity is calculated according to neoclassical expressions with the help of NCLASS code [26] with density and temperature profiles calculated by ASTRA. For simulation simplicity the radial χ_{e} dependence was ignored, $\chi_{\mathrm{e}}(r) \sim$ const. The transport coefficients were adjusted to provide consistency of the fitted density and temperature profiles and fitted plasma voltage to the experimental data. The measured and simulated density and temperature profiles are shown in figures 8(a) and (b). With the assumption of neoclassical ion thermal transport, one set of modelled transport coefficients D and χ_{e} producing consistency between the measured and simulated profiles of density and temperature, is shown in figure 9(a). In the figures the normalized minor radius is defined as a_ψ/a_{b}, where a_ψ is the half-width of a current flux surface in the midplane and a_{b} is its boundary value.

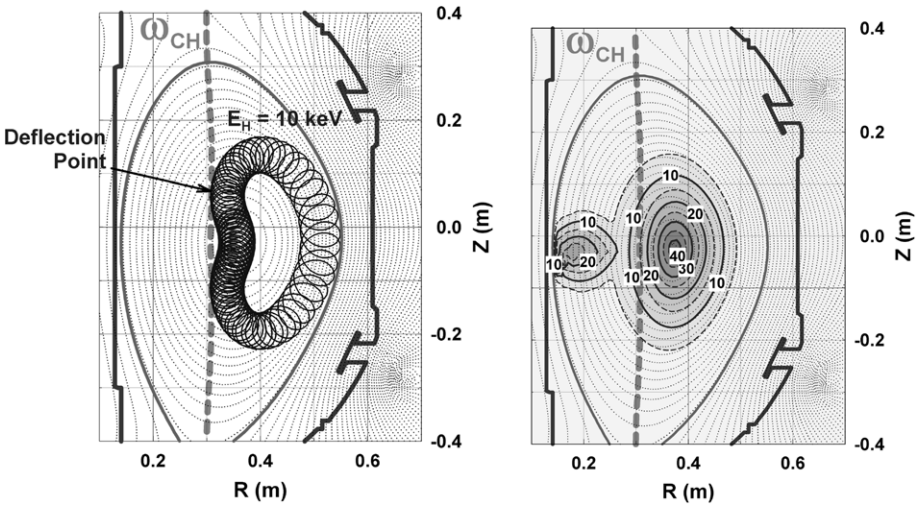

Figure 6. Left—banana trajectory of 10 keV proton inside Globus-M vacuum vessel cross section, solid fat (oval)—LCFS. Line labelled by ω_H—IC resonance position for H^+. Right—zones of different energy fast proton confinement (energy is labelled by numbers in keV). $I_p = 195$ kA, $B_T = 0.4$ T, $f_{RF} = 7.5$ MHz.

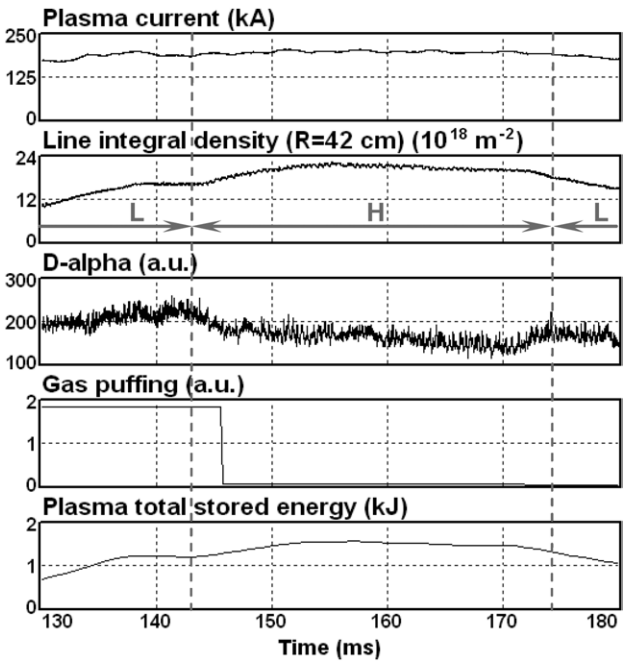

Figure 7. Time evolution of plasma parameters in OH discharge with H-mode. Shot #18083.

Plasma thermal energy content simulated by ASTRA is in good agreement with the energy content reconstructed from magnetic measurements with the EFIT code [27]. The plasma thermal energy content reached the value about 2.5 kJ, and the energy confinement time $\tau_E \sim$ 8–10 ms. This value is consistent with the ITER scaling IPB98(y,2) [28].

3.2. NBI heated H-mode and threshold power estimate

Stable L–H transition was observed during the NBI. All characteristic H-mode features are demonstrated in the NB heated H-mode, including ELMs. D-alpha and density behaviour in the NB heated H-mode discharge #19518 are shown in figure 10. For simulation of the transport processes in the NB heated H-mode the ASTRA code was also used [24]. Particle and energy sources due to NBI were calculated with the help of NBI subroutine and added in the right hand sides of corresponding equations. NBI subroutine was specially revised for the Globus-M tokamak parameters. The transport simulations were performed with the details presented in [25].

The major result of transport simulations is that common features of both ohmic and the NB heated H-modes are basically the same, i.e. large transport barrier is created on the density profile only. The particle diffusion is significantly suppressed near the transport barrier which is formed near separatrix (∼10 times) and particle diffusion coefficients fell below $D \sim 0.6\,m^2\,s^{-1}$ during both OH and NB H-modes. Ion transport did not change significantly from L to both H-mode states. It remained neoclassical with $\chi_I \sim$ 2–6 $m^2\,s^{-1}$ across the plasma radius. Strong variation was detected only in electron heat diffusivity. It changed from $\chi_e \sim 18\,m^2\,s^{-1}$ in the L-mode to $\chi_e \sim 8\,m^2\,s^{-1}$ in the NB H-mode and significantly decreased down to $\chi_e \sim 1.2\,m^2\,s^{-1}$ in the ohmic H-mode. It is worth noting that in the modelling performed not much freedom was available in the choice of an electron heat diffusivity coefficient value. The change in this coefficient from 1.2 to 5.5 $m^2\,s^{-1}$ resulted in a significant deviation of the simulated temperature profile from Thomson scattering measurements. This is illustrated in figure 9(*b*) for the ohmic H-mode regime. Rather strong discrepancy in electron heat diffusivity value between two H-mode discharges (OH and NB heated) is observed. It is in qualitative agreement with ITER IPB98(y,2) scaling, $\chi_e \sim 1/\tau_E \sim P_{tot}^{0.69}/n^{0.41}$, since in the NB H-mode density is twice as low and heating power is twice as high. Quantitative agreement is not reached yet and no adequate explanation of discrepancy between electron heat transport coefficients in H-mode regimes exists. Choosing more sophisticated radial dependence, other than $\chi_e(r) =$ const, may decrease disparity, but strong difference between two selected discharges in electron transport will be conserved.

The ASTRA code simulation revealed that the L–H transition was accompanied by an increase in the calculated electric field shearing rate in the transport barrier region. The

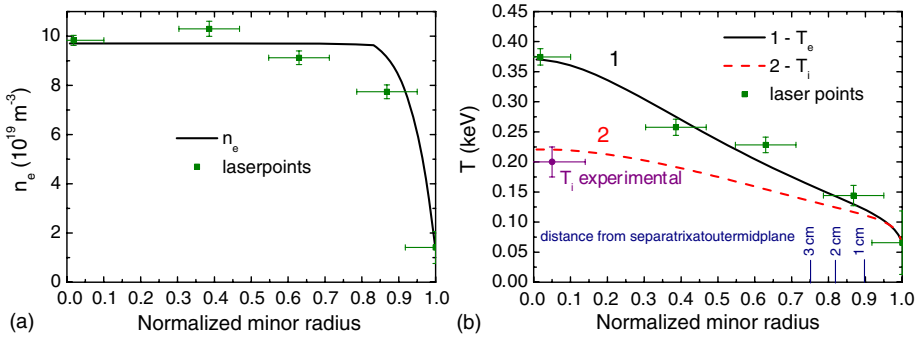

Figure 8. Measured and fitted electron density (*a*) and temperature profiles (*b*). Shot #21987, quasistationary phase of the discharge.

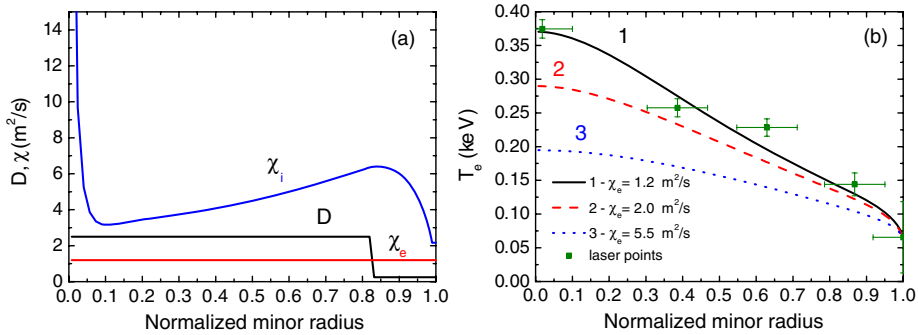

Figure 9. Left: simulated transport coefficients in ohmic H-mode. Shot #21987, quasistationary phase of the discharge. Right: effect of the electron thermal diffusivity changing in modelling on the calculated temperature profile.

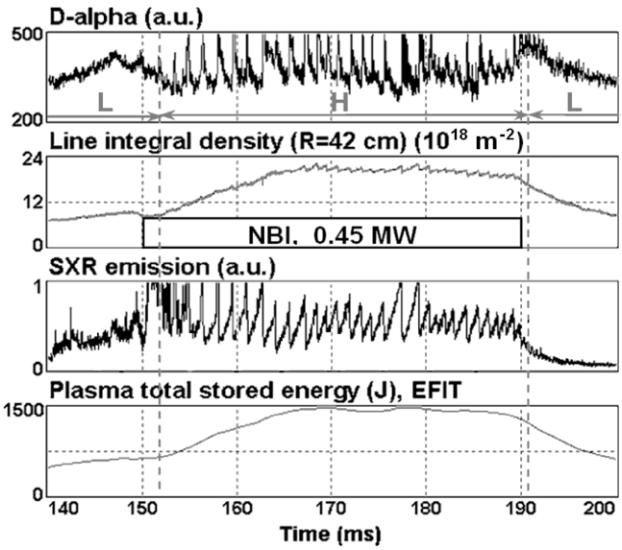

Figure 10. *L–H* transition in the NBI heated Globus-M shot #19518.

shearing rate was calculated using the neoclassical expression for the poloidal rotation without including toroidal rotation, as described in [29]. The critical shearing rate value is about $10^6\,\mathrm{s}^{-1}$, which is of the order of values typical for ASDEX-Upgrade and MAST [30]. This corresponds to the conception of the turbulent transport suppression. The *L–H* transition occurs when the heat power absorbed by ions exceeds the transition power threshold. The threshold power for the case of the Globus-M conditions calculated in accordance with the international database [28] is $P_{\mathrm{L-H}} \approx 50\,\mathrm{kW}$. In ohmic H-mode this power may be transferred to ions by electron heat flux at densities higher than $2 \times 10^{19}\,\mathrm{m}^{-3}$. That is the case for the discharge #21987. In the case of discharge #19518 the density is lower, the power flux from electrons is insufficient and auxiliary NB power absorbed by ions resolves the threshold problem. Typical power transferred to ions in the L-mode due to electron–ion exchange is below 50 kW at the densities given above in spite of relatively high ohmic power ~300 kW [25].

4. Plasma–wall interaction study

A big power flux to the first wall is a feature of the Globus-M tokamak. Keeping in mind the high power launched into discharge and power flux 'focusing' effect along the magnetic separatrix footprint the power flux density could reach several $\mathrm{MW\,m}^{-2}$ on the divertor plates. Also a small gap between plasma and the first wall in Globus-M makes plasma-facing material choice a crucial issue. At present about 90% of the in-vessel surface faced to plasma is protected with tiles manufactured from recrystallized graphite of RGTi type which is doped mainly with 2 at.% of Ti [31, 32]. Figure 11 shows the first wall picture of Globus-M. Carbo-boronization procedure based on decomposition of dodecarboran ($B_{10}C_2H_{12}$) in He glow discharge is used for vessel conditioning [33]. Boron is one of the main components of a primary protective layer deposited onto first wall surfaces and is responsible for impurity and hydrogen isotope absorption [34]. Chemical composition was analysed and structural-phase analysis was made of the deposits (mixed layers) obtained during primary carbo-boronization procedure and their following modification during plasma–wall interaction in Globus-M.

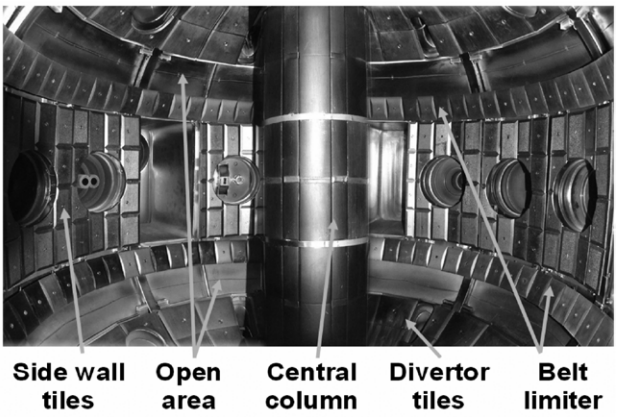

Figure 11. Plasma-facing surface (first wall) of the Globus-M vacuum vessel.

4.1. Sampling and analysis

The lower part of the Globus-M poloidal cross section with a magnetic plasma configuration enclosed is shown in figure 12(*a*). Divertor RGTi graphite tiles are marked (1–7). Part of the RGTi tiles and samples (stainless steel) were extracted from the vessel after interaction with plasma. The tiles from the zone interacting with direct plasma fluxes to the wall were exposed during ∼10 000 discharges (exposure time ∼1000 s), the stainless steel samples (probes), installed in 'shadowed' zones, were exposed to 2800 plasma discharges (exposure time ∼300 s). Electron probe microanalysis (EPMA) [35], scanning electron microscope and x-ray diffraction methods were used for the analysis. Deuterium depth profiles in layers deposited onto divertor tiles were determined by the D(^{3}He, p)^{4}He nuclear reaction in a resonance-like technique with the analysing beam of ^{3}He ions ($E = 0.69$–3.2 MeV) together with the computer program SIMNRA, simulating D atoms penetration into the deeper layers (>3 μm), inaccessible for probing ions [36, 37]. Mixed layers in 'shadowed' zone were analysed by nuclear reaction analysis with an electrostatic accelerator of deuterons ($E = 1$ MeV). Boron and carbon content in deposits were determined by comparing alpha and proton particle yields in ^{10}B(d, α)^{8}Be and ^{12}C(d, p)^{13}C reactions. Deuterium content was measured from the reaction of D(d, p)^{3}H [38–40]. Deuterium release from 'shadowed' zone samples was studied by thermodesorption spectroscopy (TDS) [41]. Residual contents of boron, carbon, silicon and titanium in the samples after their annealing during TDS and after mechanical removal of surface films were measured by the EPMA.

4.2. Divertor zone analysis results

In the zone exposed to direct plasma fluxes, RGTi divertor tiles did not suffer from destruction. At least inside 10 μm surface layer depth after 3 y of tokamak operation no structural changes were recorded. RGTi material remained in well graphitized and textured mode with a basal plane faced to plasma. Graphite matrix contained also TiC inclusions which were well identified by x-ray diffraction. All the divertor tiles which experienced direct plasma interaction were covered by mixed layers containing carbon, boron, oxygen and practically all the elements in the materials used in vessel components.

During thermodesorption analysis intensive deuterium release took place in the temperature range 600–900 K (figure 13(*a*)) which is significantly less than the initial temperature of deuterium release from RGTi graphite exposed to deuterium plasma [41]. This confirmed that deuterium was basically captured inside the mixed layers. Deuterium concentration in the divertor tile deposits was not more than 7–8 at.% (i.e. $\sim 10^{18}$ D cm^{-2}) after 10 000 tokamak pulses [42]. Minimal deuterium concentration corresponded to the maximal power flux zone. Deuterium concentration in the bulk of RGTi tiles did not exceed 2×10^{-3} at.%.

4.3. Zone 'shadowed' from direct plasma fluxes to the wall

In the 'shadowed' zones, which were recessed from direct plasma flows, most deposits had a smooth surface. Some of surfaces are rough due to inclusion of dust particles (figure 14). Deposits had a structure typical of hydrogenated amorphous carbon. Except basically amorphous carbon phase the deposit contained particles of well graphitized carbon, titanium carbide (TiC) and iron oxide (Fe_2O_3). The layers also contained main stainless steel components (Fe, Cr, Ni) as well as O, Si and Ti. Boron concentration in the deposits was lower than that of carbon. Deposits accumulated a significant amount of deuterium. The data on the deuterium accumulation in deposits are presented in table 1. The data due to nuclear resonance analysis (NRA) and thermodesorption (TDS) data are presented at the left. On the right in the same table carbon and boron areal density in mixed layers before/after annealing at 1100 K are presented measured by the EPMA.

EPMA of the annealed samples performed after thermodesorption procedure showed that the deposits were partly sublimated (table—right) and part of the deposits released as volatile compounds of deuterium with boron and carbon.

Deuterium retention estimate was made using experimental data on specific deuterium concentration measured in the different samples (table 1) and [42]. The subsequent procedure of integration over the different wall areas is quite rough and gives rather poor accuracy. Nevertheless it seems useful to provide the reader with some numbers, keeping in mind the limitation of their validity. The deuterium retention (the ratio of the total captured deuterium by the full in-vessel area to the total deuterium amount injected during the exposure time) in Globus-M is $Ret \leqslant 10\%$ [10]. In other words during each tokamak shot on average about 10% of injected deuterium is captured inside the vacuum vessel. This value fits to the database obtained from other tokamaks [43]. Comparison of the Globus-M data with the database showed that the estimated retention is closer to the values obtained at TEXTOR tokamak [44]. The approximate deuterium retention distribution between different in-vessel areas is shown in figure 12(*b*). It demonstrates that maximal deuterium trapping occurs at the divertor area.

Main processes of protective carbon–boron layer modification inside the Globus-M tokamak equipped for the first time by protection tiles manufactured from RGTi graphite are described in [10, 45, 46]. The complex mixed layers formed from protective carbon–boron layers and in-vessel component elements are amorphous and trap deuterium. The

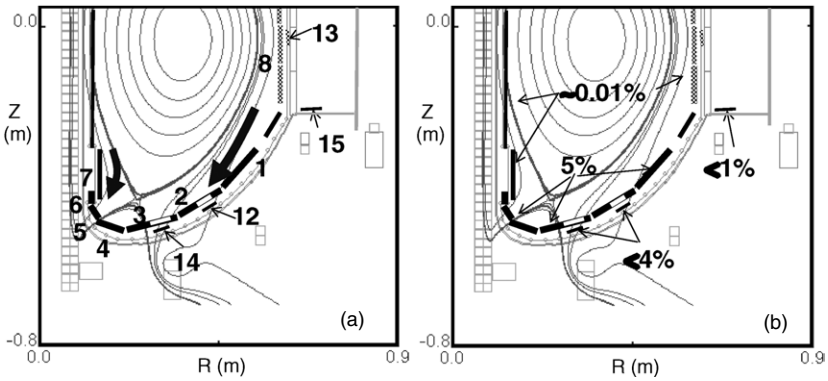

Figure 12. Cross section of the Globus-M lower part with plasma configuration enclosed. (*a*) Arrows show main fluxes to divertor tiles, divertor tiles and samples exposed to plasma are numbered. (*b*) Approximate distribution of deuterium retention across different areas of the Globus-M first wall.

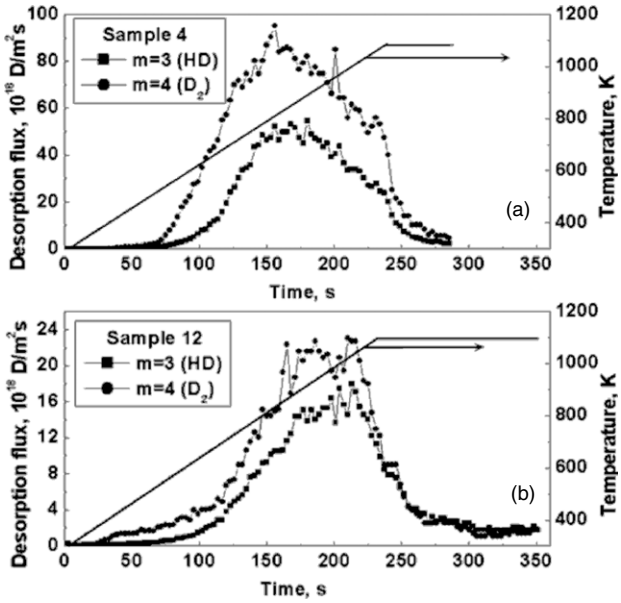

Figure 13. Deuterium thermodesorption spectra. (*a*) For the divertor tile 4. (*b*) For the deposit on sample 12. Linear heating rate is 3.2 K s^{-1}.

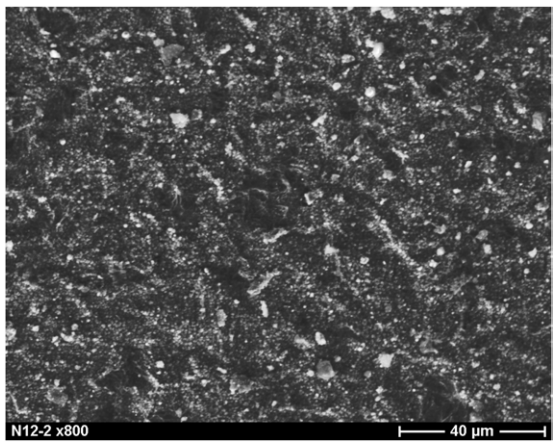

Figure 14. Scanning electron microscope micrograph of the deposit on sample 12. The deposit surface is quite rough.

Table 1. The main elements of deposited layers.

	Deuterium content (10^{16} at nm^{-2})		C (10^{16} at nm^{-2})	B (10^{16} at nm^{-2})
Sample	NRA data	TDS data (released D_2)	EPMA data before/after annealing	
12	32	46	165/80	62/31
14	31	56	86/25	23/17
15	8	15	36/10	23/16

Note: Table 1 contains corrected values for the deuterium content in samples measured by NRA, originally presented in the preprint [10].

main deuterium retention took place in the mixed layers deposited onto divertor tile surface. During heating up to 700–800 K the intensive release of hydrogen isotopes starts from the mixed layer, part of them releases together with layer components (due to 'volatility' of layers). It should be noted that temperature of deuterium release from amorphous layers is lower than temperature values specific for crystalline layers [47].

5. Central fuelling of plasma column

The fuelling method of high speed, high density plasma jet injection is developed at Globus-M. Plasma gun with explosive method of gas feeding of a coaxial accelerator permits to combine necessary merit of the fuel injector—high density and speed of the jet—with high purity of the fuel [4]. The mechanism of the jet penetration through magnetic field was proposed, and a deep penetration into tokamak plasma (far beyond separatrix) was demonstrated [5].

5.1. Experiments on high speed jet injection into Globus-M

The following jet parameters were achieved in test bench experiments: maximal density $\sim 2 \times 10^{22}$ m^{-3}, total number of accelerated particles $(1–5) \times 10^{19}$. The jet energy measured with a calorimeter increased to 200 J. The jet speed was measured by recording of jet radiation with streak camera in the visible range. The jet was imaged onto the slit photocathode oriented in parallel to the jet flow direction. Figure 15 shows the slit image swept across the slit. One can see that the plasma jet consists of several fractions, each of them propagating with its own velocity from 100 to 250 km s^{-1} according to different slopes of the strips. The presence of

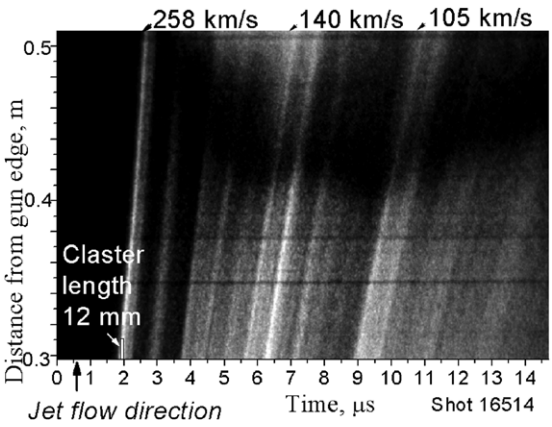

Figure 15. Streak camera sweep of the jet radiation observed through a narrow slit. The jet flow direction is from the picture bottom to top.

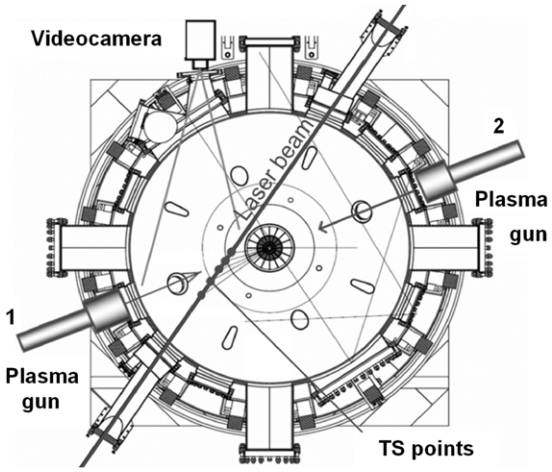

Figure 16. Horizontal cross section of the Globus-M. Fat dots indicate TS measurement points.

intensive impurity line radiation is not observed with a survey spectrometer.

Experiments on Globus-M were carried out at the following target plasma parameters: the plasma current, $I_p = 200\,\mathrm{kA}$, the toroidal field, $B_T = 0.4\,\mathrm{T}$, the average density, $\langle n \rangle = (2\text{–}5) \times 10^{19}\,\mathrm{m}^{-3}$. The plasma jet was injected from the low field side in the major radius direction, through two different ports placed in the equatorial plane (marked by 1 and 2 in figure 16). Thomson laser beam, spatial laser points at which measurements were taken and the video camera position are also shown. Port 2 is shifted by 180° in the toroidal direction from the cross section, where temperature and density were measured by Thomson scattering. Electron temperature and density profiles prior to and after jet injection into the Globus-M target plasma were measured by a high repetition rate Thomson scattering diagnostic [48, 49]. The closest in time measurements were carried out at a delay of 35 μs between jet injection and laser shot, reliable profile measurements were carried out at the delay of 50 μs. At short delay between injection and measurements, local temperature and density measurements in the case of jet injection from port 1 may be different from the values averaged over the magnetic surface. When the jet was injected from port 2 (180° toroidally from TS points), the magnetic surface averaged values were measured.

The pair of temperature and density profiles just prior to the gun shot and 50 μs after it (port 1) is shown in figure 17(*a*) (upper plots) and for port 2 figure 17(*b*) (lower plots). It is seen that already in 50 μs after the gun shot the electron density increases and temperature drops approximately twice in both cases. The target plasma density scan was made too. The jet better penetrates to the target plasma with lower density. At $n_e(0) = 5 \times 10^{19}\,\mathrm{m}^{-3}$ the temperature dropped and density grew in the central points ($R = 38.6$, 30.6 cm) more than twice in 50 μs after injection, while at $n_e(0) = 8 \times 10^{19}\,\mathrm{m}^{-3}$ the change was by 20–30% only.

5.2. *Modelling, objectives and prospects*

Jet penetration depth was estimated on the basis of the analytical model using the same approach as was developed for pellet injection simulations. The numerical simulation was performed with the code described in [7]. It is demonstrated that at $t \sim 1\,\mu$s, when the jet reaches the plasma centre the drop in the electron temperature is immense. While the electron temperature drops almost immediately, the density homogenization over the flux surface is much slower and is determined by the sound speed with the jet cloud temperature. Estimated time for the density homogenization is less than 100 μs. The penetration depth into the tokamak plasma grows with increase in the jet velocity and jet density.

During single jet injection pulse, about 20% of the injected particles are captured into tokamak plasma in Globus-M. Consequences of the plasma jet injection are strongly dependent on the injected particle fraction with respect to target plasma inventory. Too high injected particle number led to sharp rise of the target plasma density (up to three times) accompanied by even stronger temperature drop that led to the discharge disruption. At a moderate number of injected particles, the density increase up to two times was observed, accompanied by corresponding temperature drop and resulting sometimes in a locked mode development (usually $m = 2/n = 1$) followed by disruption through a sufficiently large time after injection (more than 3 ms). At a smaller jet particle number, when the density increased by no more than 50% and the temperature dropped no more than twice, the plasma remained MHD stable. In all three cases, the Thomson measurements and video camera observations prove that the jet penetrated to the plasma centre. Consequently a right choice of the jet parameters makes it possible to grow the column particle number and control the density profile in a discharge, realizing the main particle contribution to the central or peripheral zone. No essential impurities coming in either with the jet, or due to its interaction with tokamak injection port, were recorded. The jet injection at the right choice of the jet parameters did not affect the global characteristics of the tokamak discharge such as plasma current and loop voltage.

Analogy may be made between the plasma jet and pellet injection. In both cases, the penetration ability depends on speed and density of the injected object, and the influence degree to the target plasma is defined by total number of injected particles. At that, decrease in the particle density in the plasma jet (10^{21}–$10^{22}\,\mathrm{m}^{-3}$) by one to two orders of

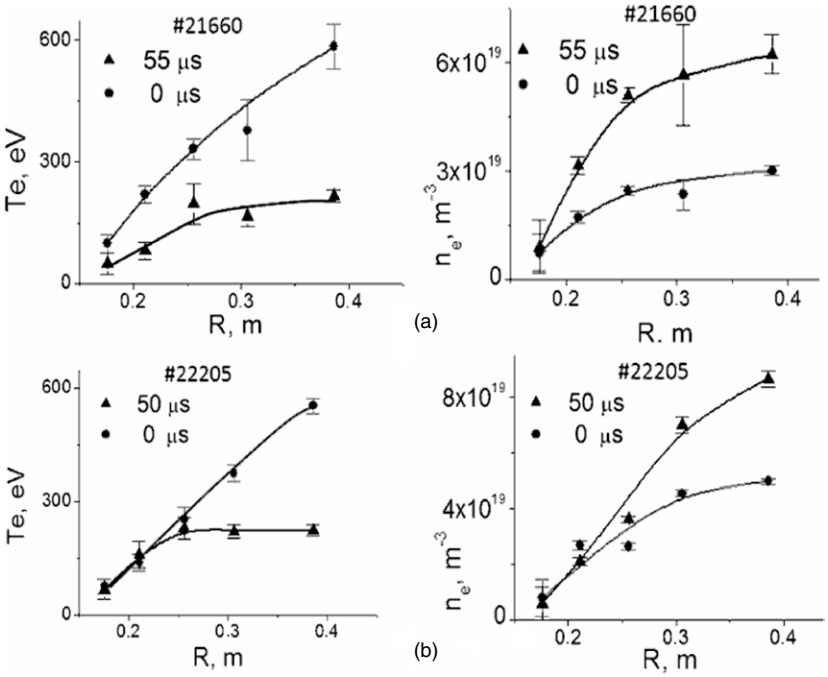

Figure 17. Electron density and temperature profiles measured before and shortly after the jet injection, in cross section near the gun (upper row, shot #21660) and in remote cross section (lower row, shot #22205).

magnitude in comparison with the particle density in the cloud surrounding the pellet (10^{23}–10^{24} m^{-3}), is compensated by the corresponding velocity increase. During a pellet injection spreading of gas cloud along the magnetic field takes place [50]. In the plasma jet injection experiments also the gas cloud spreading effect along the magnetic field lines is detected and coincidence of the shape of protuberances spreading along magnetic field with the pitch angle and curvature of the field lines in the central region of the plasma is shown [51].

6. Conclusions

During auxiliary heating at Globus-M MHD stable plasma regimes with high value of specific energy content (up to 8 kJ m^{-3}) and high beta normalized ($\beta_N \approx 6\%$ m T MA^{-1}) were achieved at moderate heating power (<0.8 MW). Fast particle behaviour was investigated and their generation, confinement and slowing down in the conditions of low magnetic field during the NBI and ICRH was clarified. An important feature is that most of the investigations were performed at low values of the edge safety factor, which is unusual for STs, $2.7 < q_{95} < 5$ and small plasma–outer wall gap (3–5 cm). Reliable transition to the H-mode regime was obtained. The different types of H-modes are accessed (ohmic, NB heated, etc) and the threshold power was found to be in accordance with the international database. Large transport barrier was created for the density and significant diffusion coefficient drop (∼10 times) was testified by the ASTRA transport code in the vicinity of the separatrix. Experience of the RGTi graphite utilization in the Globus-M ST is positive and connected with its high density, low erosion coefficient and poor deuterium sorption ability. A tool for central plasma fuelling on the basis of dense, high velocity plasma jet injection is developed at Globus-M. Injection of the jet with velocity of 200 km s^{-1} leads to nearly instantaneous increase in density in the centre of the plasma column. The plasma density increase is recorded on the magnetic axis of target plasma with 0.2 MA current and density of (2–5) × 10^{19} m^{-3} within 35–50 μs after injection started. At the same time electron temperature drops significantly.

Acknowledgments

The authors regret that during the preparation of this paper the famous plasma physicist Victor Golant passed away.

The authors would like to thank A Polevoy and G Pereversev for their help in ASTRA simulations. This work is supported by the Russian Academy of Sciences, Ministry of Science and Education, Rosatom (contract H.4a.41.03.08.075), the IAEA Research Agreement 14720 and RFBR grants ## 06-02-08142, 06-02-16709, 06-02-08186, 06-02-16189, 06-03-32854, 06-08-00878, 07-02-13557, 08-02-00511, 08-02-01313, 08-02-00992, 0802-13537-ofi-c, 08-02-13530-ofi-c.

References

[1] Gusev V.K. *et al* 1999 *Tech. Phys.* **44** 1054
[2] Irzak M.A. *et al* 1999 *Plasma Phys. Rep.* **25** 659
[3] Gusev V.K. *et al* 2004 *Tech. Phys. Lett.* **30** 690
[4] Voronin A.V. *et al* 2005 *Nucl. Fusion* **45** 1039–45
[5] Gusev V.K. *et al* 2006 *Nucl. Fusion* **46** S584–91
[6] Shcherbinin O.N. *et al* 2006 *Nucl. Fusion* **46** S592–77
[7] Rozhansky V. *et al* 2006 *Nucl. Fusion* **46** 367–82
[8] Gusev V.K. *et al* 2006 *Proc. 21st Int. Conf. on Fusion Energy 2006 (Chengdu, China, 2006)* (Vienna: IAEA) CD-ROM file OV/P-3 and http://www-naweb.iaea.org/napc/physics/FEC/FEC2006/html/index.htm
[9] Ayushin B.B. *et al* 2008 *Plasma Phys. Rep.* **34** 81–94

[10] Gusev V.K. *et al* 2009 In-vessel surface layer evolution during plasma–wall interaction in the Globus-M spherical tokamak *Nucl. Fusion* **49** at press
[11] Gusev V.K. *et al* 2007 *Tech. Phys.* **52** 1127
[12] Akers R.J. *et al* 2002 *Nucl. Fusion* **42** 122–35
[13] Cox M. *et al* 1999 *Fusion Eng. Des.* **46** 397–404
[14] Ono M. *et al* 2000 *Nucl. Fusion* **40** 557–61
[15] Izvozchikov A.B. *et al* 1992 *Tech. Phys.* **37** 201
[16] Chernyshev F.V. *et al* 2008 *Proc. 35th EPS Plasma Phys. Conf. (Hersonissos, Crete, Greece, 9–13 June 2008)* P-2.097 http://epsppd.epfl.ch/Hersonissos/pdf/P1_151.pdf
[17] Sigmar D.J. 1980 *Varenna Course on Physics of Plasmas Close to Thermonuclear Conditions* vol 1 (Brussels, Belgium) p 271
[18] Chernyshev F.V. *et al* 2007 *Proc. 34th EPS Conf. on Plasma Phys. (Warsaw, Poland, 2–6 July 2007)* **31F** (ECA) P-5.107 http://epsppd.epfl.ch/Warsaw/pdf/P5_107.pdf
[19] Lao L.L. *et al* 1985 *Nucl. Fusion* **25** 1611
[20] Ayushin B.B. *et al* 2007 *Proc. Zvenigorod Conf. on Plasma Physics and Controlled Fusion (Zvenigorod, Russia, 12–16 February 2007)*
[21] Stix T.H. 1975 *Nucl. Fusion* **15** 737–54
[22] Chaniotakis E.A. and Sigmar D.J. 1993 *Nucl. Fusion* **33** 849–61
[23] Gusev V.K. *et al* 2007 *Proc. 34th EPS Conf. on Plasma Phys. (Warsaw, Poland, 2–6 July 2007)* **31F** (ECA) P-1.078 http://epsppd.epfl.ch/Warsaw/pdf/P1_078.pdf
[24] Pereverzev G. and Yushmanov P. 2002 *Max-Plank IPP Report* 5/98
[25] Senichenkov I. Yu *et al* 2008 *Proc. 35th EPS Plasma Physics Conf. (Hersonissos, Crete, Greece, 9–13 June 2008)* P-2.046 http://epsppd.epfl.ch/Hersonissos/pdf/P2_046.pdf
[26] Houlberg W.A. *et al* 1997 *Phys. Plasmas* **4** 3230
[27] Gusev V.K. *et al* 2006 *Tech. Phys.* **51** 987
[28] Doyle E.J. *et al* 2007 ITER Physics Basis *Nucl. Fusion* **47** S18
[29] Sakharov N.V. *et al* 2008 *Proc. 22nd Int. Conf. on Fusion Energy 2008 (Geneva, Switzerland 2008)* (Vienna: IAEA) CD-ROM file EX/P5-16 and http://www-naweb.iaea.org/napc/physics/FEC/FEC2008/html/index.htm
[30] Rozhansky V. 2006 *Contrib. Plasma Phys.* **46** 575
[31] Burtseva T.A. *et al* 1993 *Carbon Materials, Proc. 6th Int. Workshop (Jülich, Germany, 23–24 September 1993)* p 49
[32] Gorodetsky A.E. *et al* 1998 *Fus. Eng. Des.* **43** 129
[33] Sharapov V.M. *et al* 1995 *J. Nucl. Mater.* **220–222** 730
[34] Alimov V. Kh *et al* 1992 *J. Nucl. Mater.* **196–198** 670
[35] Zalavutdinov R. Kh *et al* 1994 *Microchim. Acta* **114–115** 533
[36] Alimov V. Kh *et al* 2005 *Nucl. Instrum. Methods.* B **234** 169
[37] Mayer M. 1997 *SIMNRA User's Guide, Technical Report IPP 9/113*, Garching, www.rzg.mpg.de/∼mam
[38] Tesmer J.R. *et al* 1995 *Handbook of Modern Ion Beam Materials Analysis* (Pittsburgh, PA: Materials Research Society)
[39] Gavrilov G.E. *et al* 2003 *Nucl. Instrum. Methods.* A **515** 108
[40] Brazhkin V.V. *et al* 2006 *Phys. Rev.* B **74** 140502-1 (rapid communications)
[41] Arkhipov I.I. *et al* 1999 *J. Nucl. Mater.* **271–272** 418
[42] Gusev V.K. *et al* 2007 *Proc. ICFRM-13* 000390 *(Nice, France, 10–14 December 2007)* p 823 http://www-fusion-magnetique.cea.fr/icfrm13/cd/data/index.html
[43] Lipschultz B. *et al* 2007 *Nucl. Fusion* **47** 1189–205
[44] Wienhold P. *et al* 2003 *J. Nucl. Mater.* **313–316** 311
[45] Ananiev A.S. *et al* 2002 *Semiconductors*. **36** 941–3
[46] Sakharov N.V. *et al* 2002 *Proc. 29th EPS Conf. on Plasma Physics and Controlled Fusion (Montreux, Switzerland, 17–21 June 2002)* P—5.078 http://epsppd.epfl.ch/Montreux/pdf/P5_078.pdf
[47] Kikuchi Y. *et al* 2007 *Proc. 13th Int. Conf. on Fusion Reactor Materials (Nice, France, 2007)* p 3790 http://www-fusion-magnetique.cea.fr/icfrm13/cd/data/index.html
[48] Tolstyakov S. Yu *et al* 2006 *Tech. Phys.* **51** 846–52
[49] Tolstyakov S. Yu *et al* 2008 *Proc. 35th EPS Plasma Physics Conf. (Hersonissos, Crete, Greece, 9–13 June 2008)* P.2-108 http://epsppd.epfl.ch/Hersonissos/pdf/P2_108.pdf
[50] Pegourie B. 2007 *Plasma Phys. Control. Fusion* **49** R87–160
[51] Petrov Yu V. *et al* 2008 *Proc. 22nd IAEA Fusion Energy Conf. (Geneva, Switzerland, 13–18 October 2008)* EX/P5-8 http://www.fec2008.ch/preprints/ex_p5-8.pdf